# Fouling reduction of reverse osmosis membrane by surface modification via layer-by-layer assembly

Toru Ishigami, Kuniaki Amano, Akihiro Fujii, Yoshikage Ohmukai, Eiji Kamio, Tatsuo Maruyama, Hideto Matsuyama *

Center for Membrane and Film Technology, Department of Chemical Science and Engineering, Kobe University, 1-1 Rokkodai, Nada-ku, Kobe 657-8501, Japan

ABSTRACT

To reduce membrane fouling of reverse osmosis (RO) membrane, we adopted layer-by-layer (LbL) assembly. LbL assembly has received attention as a means of preparing ultrathin layers of composite membranes. In addition, it can suppress membrane fouling due to its hydrophilicity. In this study, we deposited polyelectrolytes on a commercial RO membrane via LbL assembly and especially investigated the effect of layer number on membrane properties. The obtained membranes exhibited antifouling properties, such as high water permeability and high ion rejection, against various hydrophobic foulants. In addition, membrane hydrophilicity increased and surface roughness became smooth as layer number increased. We also found an optimum layer number that admitted highest water permeability. Quartz crystal microbalance with dissipation measurements revealed that the polyelectrolyte multilayer indeed suppresses foulant adsorption. Protein conformational change was low on the polyelectrolyte film surface, compared with that on the polyamide layer.

© 2012 Elsevier B.V. All rights reserved.

## 1. Introduction

Seawater desalination process with reverse osmosis (RO) membrane has been widely used and supplied high quality water. The main RO membrane in current use is a polyamide composite membrane with high water permeability and high ion rejection. During operation, the water permeability of the membrane decreases over time due to membrane fouling. When this happens, the membrane must be replaced, and surplus pump power to supply the seawater is also required. Thus, a viable means of improving the energy expenditure and reducing the cost of the seawater desalination process is to improve the antifouling properties of currently available RO membranes. Previous studies have indicated that surface roughness [1,2], initial permeate flux [3], surface charge [4], hydrophobic interactions between the polyamide and some organic foulants [5–9] are responsible for serious fouling. To solve this problem, a number of methods to modify RO membrane surfaces have been developed and reported. Surface modification by graft polymerization of hydrophilic molecules such as polyethylene glycol prevents the adsorption of the organic foulants such as proteins or surfactants and improves the antifouling capability [10–12]. However, ease of operation of these methods is limited by their requirement for multistep operations such as graft polymerization.

Layer-by-layer (LbL) assembly is an attractive method for preparing the ultrathin layer of composite membranes. In this method, a polycation and a polyanion are alternately deposited on a substrate and are adsorbed by electrostatic interaction. Advantages of LbL are that film thickness can be controlled at the nanometer scale [13,14] to allow for high water flux. Further, film properties can be optimized by varying kinds of polyelectrolytes [15,16] and deposition conditions [17,18]. The surface charge of the film can be either positive or negative depending on whether the outer film is specified with a polycation or polyanion [19]. The membrane surface with rough morphology can be smoothed by polyelectrolyte deposition. In addition, recent studies have reported the existence of polyelectrolyte multilayered membranes which are biocompatible and hydrophilic [20–22]. LbL assembly is therefore expected to suppress membrane fouling of RO membranes appreciably.

A few research groups have applied the principles of LbL assembly to membrane separation processes, for instance, to nanofiltration (NF) [23], pervaporation [24,25] and gas separation [26]. Of particular interest, Bruening et al. successfully prepared an NF membrane by LbL assembly and studied its charge density, permeability and rejection performance in detail [16,27]. Tung et al., performed the depth profile characterization of multilayered NF membranes by positron annihilation spectroscopy [28]. In addition, a few research groups have applied LbL assembly to substrates [29,30] and NF membranes [31,32] to improve fouling resistence. However, to our knowledge, there have been no equivalent investigations on the application of LbL assembly to RO membranes and on

* Corresponding author. Tel./fax: +81 78 803 6180.
E-mail address: matuyama@kobe-u.ac.jp (H. Matsuyama).

its potential to improve the antifouling properties of such membranes.

The aim of this study was to improve the antifouling property of RO membranes by modifying their surfaces via LbL assembly. The key issue of polyelectrolyte deposition on RO membranes is not only to suppress the membrane fouling, but also to retain, as far as possible, the water permeability and ion rejection capabilities of RO membrane used as substrate. The LbL assembly process is expected to decrease initial water permeability, although the antifouling property and ion rejection capacity may improve as number of layers increases. Thus, in this study, we aimed for preparation of an RO membrane with higher final water permeability (after fouling) than that of the original commercial RO membrane. In addition, we investigated the effect of layer number on the water permeability, sodium chloride (NaCl) rejection and the antifouling capability of the membrane.
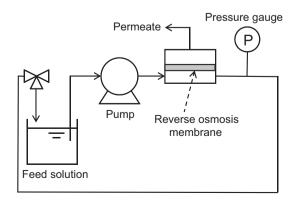
## 2. Experimental

### 2.1. Materials

Poly(sodium 4-styrenesulfonate) (PSS, Mw = 70 kDa) and poly(allylamine hydrochloride) (PAH, Mw = 70 kDa) were obtained from Sigma–Aldrich and used without further purification. NaCl was also used as-received. The pH of polyelectrolyte solutions was adjusted with dilute hydrochloric acid. Bovine serum albumin (BSA) (Aldrich Chemical, WI), humic acid and dodecyl trimethyl ammonium bromide (DTAB) were sourced from Wako Pure Chemical Industries, Aldrich Chemical and Tokyo Chemical Industries, respectively, and used without further purification. The substrate for the experiments was a commercial RO membrane (ES-20; Nitto Denko, Japan). M-phenylene diamine (MPD), isophthaloyl dichloride (IPC) and acetone and N-methyl pyrrolidone (NMP) were used to synthesize the polyamide polymer required for the measurement of quartz crystal microbalance with dissipation (QCM-D).

### 2.2. Film deposition on RO membrane

Polyelectrolyte was deposited on the RO membrane in a cross flow apparatus as shown in Fig. 1. Polyelectrolyte solution of concentration $10 \, \text{g L}^{-1}$ were prepared by dissolving polyelectrolyte with 1 M NaCl in 10 mM Tris buffer. The pH of polyelectrolyte solutions was adjusted to 7.0. PAH and PSS solutions were alternatively supplying to the membrane surface for 30 min. Prior to supplying next polyelectrolyte solution, the membrane surface was rinsed for 5 min with Milli-Q water. The multilayered polyelectrolyte film were grown by repeating these adsorption cycle (to achieve the desired number of polyelectrolyte layers). The operating pressure

and the flow rate were set to 0.75 MPa and $1.0 \, \text{mL min}^{-1}$, respectively. The feed side of the membrane cell was stirred at 500 rpm by a magnetic stirrer. PSS and PAH were adsorbed to the outer surface of the membrane in the case of even numbered layer and odd numbered layer, respectively.

### 2.3. Characterization of film deposition on RO membrane

#### 2.3.1. SEM observation

To obtain dry membranes, the membranes were placed in a freeze dryer (FD-1000; EYELA, Japan) for 15 h. The dry RO membranes were fractured in liquid nitrogen and sputtered with Pt/Pd. The outer surfaces of the membranes were examined under a scanning electron microscope (JSM-5610LVS; Hitachi, Japan) with an accelerating voltage of 15 kV.

#### 2.3.2. AFM observation

As with the SEM analyses, the surface morphology of the membranes was observed with an atomic force microscope (SPI3800N/SPA400, SII, Japan) in tapping mode. From AFM analyses of the RO membranes, surface roughness was quantitatively determined. The mean roughness ($R_a$) is the mean value of surface relative to the center plane and is calculated as follows:

$$R_a = \frac{1}{L_x L_y} \int_0^{L_x} \int_0^{L_y} |f(x,y)| \, dx \, dy \tag{1}$$

where $f(x, y)$ is surface relative to the center plane and $L_x$ and $L_y$ are surface dimensions.

#### 2.3.3. Zeta potential measurement

The zeta potential of polyelectrolyte multilayer film on the RO membrane was determined by electrophoretic mobility with an electrophoretic measurement apparatus (ELS-6000; Otsuka Electronics, Japan) using a plate sample cell. Polystyrene latex particles (Otsuka Electronics, Japan, diameter 520 nm) coated with hydroxypropyl cellulose (HPC, Scientific Polymer Products, Japan, Mw = 300,000) were used as mobility-monitoring particles. These particles were dispersed in a 10 mM NaCl solution to prevent interactions with the quartz cell surface during measurement. Zeta potential measurements were conducted with membrane samples in a background solution of 10 mM NaCl at pH 5.5 [33].

#### 2.3.4. Air bubble contact angle measurement

To evaluate the degree of membrane hydrophilicity, air bubble contact angle measurements were performed using a contact angle meter (CA-A, Kyowa Interface Science, Japan). Air bubbles were injected onto the under surface of the polyelectrolyte multilayer immersed in the water chamber. Each contact angle was measured 10 times and an average value was calculated.

#### 2.3.5. Filtration experiment

The filtration experiment was carried out using the same cross-flow type module as was used in the film deposition experiment. NaCl solution ($500 \, \text{mg L}^{-1}$) comprised the feed solution for salt rejection measurements. BSA, humic acid and DTAB solution (each $50 \, \text{mg L}^{-1}$) comprised the feed solutions for the fouling experiments. DTAB is not common foulant, but it was used to investigate the effect of cationic organic compound on membrane fouling. The pH of solutions was adjusted to 7.0. Each feed solution was pumped to the polyelectrolyte multilayered RO membrane in the module. The feed side of the membrane cell was stirred at 500 rpm by a magnetic stirrer. The trans-membrane pressure was set to 0.75 MPa by adjusting a pressure valve close to the retention side, and the pressure was averaged from several readings of the pressure gauge. For each filtration experiment, deionized (DI) water was first



**Fig. 1.** Schematic diagram of the polyelectrolyte deposition and the filtration experiments using the membrane module.

permeated as a feed and the initial water permeability $J_0$ [L m$^{-2}$ h$^{-1}$ atm$^{-1}$] was measured. Then feed solution was filtered and the permeability, $J$ [L m$^{-2}$ h$^{-1}$ atm$^{-1}$] was measured. Each datum of water permeability is the average of three independent measurements .

NaCl rejection $R$ [%] is defined as

$$R = \left(1 - \frac{C_p}{C_f}\right) \times 100 \tag{2}$$

where $C_f$ [wt.%] and $C_p$ [wt.%] represent the NaCl concentration in feed and permeate solution, respectively. The BSA concentrations in the feed and permeate solution were measured at 280 nm by a U-2000 UV spectrophotometer (Hitachi Co., Japan).

### 2.4. Quartz crystal microbalance with dissipation (QCM-D) measurement

#### 2.4.1. Preparation of the polyamide and the polyelectrolyte multilayer on the quartz crystal sensor

In the present study, the polyamide layer and the polyelectrolyte multilayer were deposited on a sensor composed of gold-coated AT-cut quartz crystals (Qsense AB, Gothenburg, Sweden) [34]. A polyamide layer of commercial RO membrane is usually synthesized by interfacial polymerization with m-phenylenediamine (MPD) as diamine and trimesoyl chloride (TMC) as acid chloride [35,36]. However, these highly cross-linked polyamides do not dissolve in solvent, and hence cannot be coated onto the quartz crystal sensor. In our study, isophthaloyl dichloride (IPC) was substituted for TMC to synthesize a polyamide without cross-linking. Actually, the polyamide synthesized with IPC was different from that with TMC. The polyamide synthesized with IPC is a linear structure, while that with TMC is the cross-linked structure [37]. However, the interfacial properties may be similar, because the repeating unit structure of the polyamide synthesized with IPC is same as that with TMC. Thus, the effect of the polyelectrolyte multilayered deposition can be investigated because both of them have similar molecular structures. To prepare the polyamide, 1.80 g sodium hydroxide was dissolved in 100 mL MPD solution. This solution was blended with 100 mL IPC solution. The resulting mixture was stirred for 1 h at 323 K and dried overnight at 333 K. This procedure yielded a non-cross-linked polyamide of average molecular weight $1.26 \times 10^5$, which was then dissolved in NMP. The polyamide solution (1 wt.%) was spin-coated on the quartz crystal sensor for 1 min at 2000 rpm and dried for 30 min at 343 K. Finally, to prepare the polyelectrolyte multilayered quartz crystal sensor, PAH and PSS solutions were alternately supplied to the polyamide layer on the sensor until 6 layers had been deposited.

#### 2.4.2. Measurements of the adsorption amount and the viscoelasticity of adsorbed layer

The QCM-D technique relies on a sensor comprising a piezoelectric quartz crystal oscillating in a shear mode. An increase in adsorbed mass on the QCM sensor surface induces a decrease in resonance frequency. In the case of a thin nondissipative adsorbed layer with no-slip boundary condition, the adsorbed mass, $\Delta m$ [ng cm$^{-2}$] is directly proportional to the frequency shift, $\Delta f$ [Hz], through the Sauerbrey equation [38]:

$$\Delta m = -C\frac{\Delta f}{n} \tag{3}$$

where the mass sensitivity constant is denoted $C$ (17.7 ng cm$^{-2}$ Hz$^{-1}$ for a 5 MHz crystal), and $n$ [–] (1, 3, 5) is the overtone number. The 3rd overtone (15 MHz) was chosen whenever the Sauerbrey equation was employed in the data analysis. In addition to the frequency shift, the dissipation factor, $D$ [–], was also monitored. $D$ is defined as

$$D = \frac{E_{\text{lost}}}{2\pi E_{\text{stored}}} \tag{4}$$

where $E_{\text{lost}}$ [J] is the energy dissipated during each oscillation cycle, and $E_{\text{stored}}$ [J] is the total energy of the system. For Eq. (3) to be valid the dissipation value $\Delta D$ [–] is required to be low, which is the case in this study.

The experiments were begun by verifying the stability of both the resonance frequency and the dissipation of the sensor in PBS buffer. Next, BSA solution (50 mg L$^{-1}$) were supplied to the sensor and the frequency and the dissipation changes were followed over time. All quartz crystal sensors applied in the QCM-D studies were ozone-cleaned for 30 min before use (UV/Ozone ProCleaner; Bioforce Nanosciences, IA), to remove any hydrocarbon contamination layers. Each experiment was performed at 298 K under static conditions, and repeated 3–5 times to ensure good statistics.
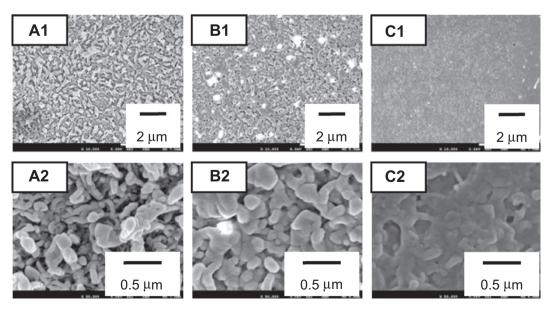


**Fig. 2.** SEM images of polyelectrolyte multilayered RO membrane. (A) 0-Layered (original RO membrane). (B) 6-layered. (C) 12-Layered. 1: Outer surface. 2: Magnified outer surface.
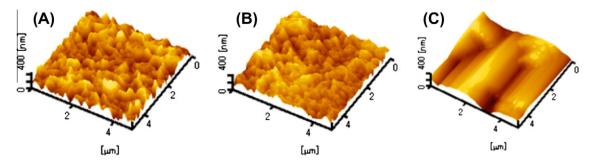
**Fig. 3.** AFM images of outer surface of polyelectrolyte multilayered RO membrane. (A) Un-layered (original RO membrane). (B) 6-Layered. (C) 12-Layered.

**Table 1**
Effect of layer number on mean roughness of the outer surface of polyelectrolyte multilayered RO membranes.[a]

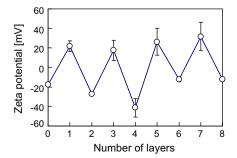| Membrane | $R_a$ (nm) |
|---|---|
| Original RO membrane | 54.9 |
| 6-Layered RO membrane | 44.0 |
| 12-Layered RO membrane | 34.8 |

[a] $R_a$: mean roughness.

## 3. Results and discussion

### 3.1. Membrane formation and its characterization

Fig. 2 shows the SEM images of outer surfaces of the polyelectrolyte multilayered RO membranes compared with the original commercial RO membrane. AFM images of these membranes are displayed in Fig. 3. On the original commercial RO membrane, the rough surface morphology known as specific structure of RO membrane is clearly visible (Fig. 2A1 and A2). The surface structure becomes smooth as the number of layers increases (Figs. 2B1, C1, Fig. 3B and C). In the 6-layer case, it is seen that the multilayered RO membrane surface is covered with a thin layer (Fig. 2B2). As the number of layers increases to 12, the multilayered surface is further covered with polyelectrolytes and the valley parts of the rough morphology are filled in with the deposition (Fig. 2C2). Table 1 shows the relationship between the layer number and the mean roughness $R_a$ of polyelectrolyte multilayered RO membranes. This indicates that the roughness decreases significantly as the number of layers increases. This result is consistent with the SEM result. The smoothed surface morphology is expected to improve the antifouling capability of the polyelectrolyte multilayered RO membrane.

Fig. 4 shows the relationship between the layer number and the zeta potential of polyelectrolyte multilayered RO membranes. Here, zeta potential starts from about –18 mV, indicating that the

original RO membrane is negatively charged. The surface charge becomes positive after the adsorption of PAH, and reverts to negative after PSS adsorption. The observed behavior of the alteration of the surface charge with addition of oppositely charged polyelectrolytes is similar to that known for polyelectrolyte adsorption [36,39–41].

Fig. 5 shows the relationship between the layer number and the air bubble contact angle. From this figure, it is seen that the air bubble contact angle increases as layer number increases. Thus, it was found that the film surface becomes hydrophilic as the layer number increases. Essentially, polyelectrolyte deposition renders the membrane surface more hydrophilic because the polyelectrolytes are water-soluble polymers. The correlation of adsorption behavior of polyelectrolyte with the surface charge density has been described in previous papers [13,42]. In short, with increasing layer number, the polyelectrolytes form loops and tails, and the surface charge density also increases. This increase of the charge density may further increase the hydrophilicity. The enhanced hydrophilicity is also expected to improve the antifouling capability of RO membrane.

From these SEM, zeta potential and contact angle measurements, we could confirm that polyelectrolytes were successfully deposited onto the original RO membrane.

### 3.2. Filtration experiment

Fig. 6 shows the effect of layer number on water permeability and NaCl rejection after 120 min filtration, obtained from the filtration experiment with NaCl solution. As the layer number increases, water permeability decreases while NaCl rejection increases. These trends result because the hydrodynamic resistance and the effective mass diffusivity in the polyelectrolyte multilayered RO membrane increases and decreases, respectively, due to the increasing layer thickness. Thus, the performance of the polyelectrolyte multilayered RO membrane can be controlled by changing the layer number.
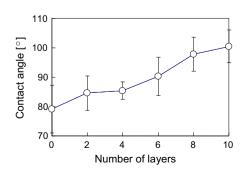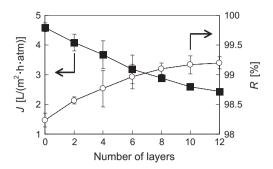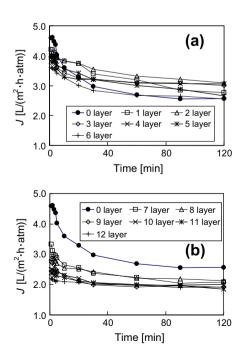


**Fig. 4.** Change of zeta potential of polyelectrolyte multilayered RO membrane with increase of layer number.



**Fig. 5.** Effect of layer number on air bubble contact angle of polyelectrolyte multilayered RO membrane.

**Fig. 6.** Effect of layer number on water permeability $J$ (black squares) and NaCl rejection (unfilled circles) of polyelectrolyte multilayered RO membrane.



**Fig. 8.** Effect of layer number on water permeability (unfilled circles) and relative permeability (black squares) of polyelectrolyte multilayered RO membrane after 120 min filtration with BSA solution.

Fig. 7 shows the time variation of the water permeability of the original and the polyelectrolyte multilayered RO membrane, obtained from the filtration experiment with BSA solution. Water permeabilities after 120 min settle into a near-steady-state for all layer numbers. Severe decreases in water permeability of the original RO membrane occur within the first 20 min of testing. On the other hand, water permeabilities of the polyelectrolyte multilayered membrane gradually decline although the initial water permeabilities are lower due to the layer deposition. Importantly, the water permeabilities of the layered membranes (1–6 layers) after 60 min were higher than that of the original membrane. These effects are even more dramatic when 7–12 layers are applied (Fig. 7b).

Fig. 8 shows the permeability and the relative permeability versus layer number after 120 min filtration with BSA solution. Relative permeability is defined as the permeability at 120 min, $J$ divided by the initial water permeability, $J_0$. From the relative permeabilities, it was found that the antifouling capability is improved with increasing layer number. This occurs because the membrane surface becomes hydrophilic and the surface roughness becomes smooth with increasing layer number, as described above. On the

other hand, the true water permeability increases up to 4 layers and then declines, as the increased hydrodynamic resistance in the thicker assembled layers compensates the antifouling improvement. In addition, it is seen that the water permeability of an even numbered layer is higher than those of its preceding and successive odd number layers. BSA, with isoelectric point 4.8 [43], is negatively charged in the feed solution at pH = 7. The adsorption of negatively charged BSA onto the negative charged surface is suppressed by electrostatic repulsion in addition to enhanced hydrophilicity on the membrane surface in the case of an even numbered layer. On the other hand, for odd numbered layers, the contributions to the antifouling capability are hydrophilicity enhancement on the membrane surface and surface smoothing. Thus, the antifouling capability is more pronounced when even numbers of layers are applied to the original membrane surface.

Figs. 9 and 10 show the time variation of the water permeability of the original and the polyelectrolyte multilayered RO membrane, obtained from the filtration experiment with humic acid solution and DTAB solution, respectively. As observed for the experiment with BSA solution, water permeabilities of the original RO membrane dramatically decline with time. In contrast, the water permeabilities of the polyelectrolyte multilayered membranes decrease more gradually as layer number increases. As can be seen in Fig. 10, the final water permeabilities of any even-layered membranes are higher than those of the original RO membrane, despite DTAB being a cationic surfactant and the outer surface of polyelectrolyte multilayered membrane having a negative charge. This implies that LbL assembly on membrane surface is useful for fouling reduction not only in the case of electrostatic repulsion between foulant and membrane surface but also in the case of electrostatic attraction.



**Fig. 7.** Time variation of the water permeability of the original and the polyelectrolyte multilayered RO membrane with BSA solution. (a) Original RO membrane (0-layer) and polyelectrolyte multilayered membrane with 1–6 layers. (b) Original RO membrane and polyelectrolyte multilayered membrane with 7–12 layers.
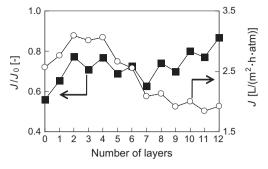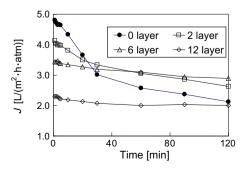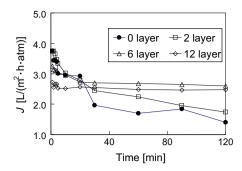


**Fig. 9.** Time variation of the water permeability of the original (0-layer) and the polyelectrolyte multilayered RO membrane (2, 6 and 12 layers) with humic acid solution.

**Fig. 10.** Time variation of the water permeability of the original (0-layer) and the polyelectrolyte multilayered RO membrane (2, 6 and 12 layers) with DTAB solution.



**Fig. 12.** Dissipation change, $\Delta D$, as a function of frequency change, $\Delta f$, during BSA adsorption onto un-layered and 6-layered polyamide-coated QCM sensor.

### 3.3. QCM-D result for protein adsorption

Time variations of the amount of adsorbed BSA onto polyelectrolyte un-layered and 6-layered polyamide-coated quartz crystal sensor are shown in Fig. 11. The time at which BSA solution was first supplied is set to zero. The amount of BSA adsorbed onto the QCM sensor increases up to adsorption equilibrium in both cases. The surface mass densities of adsorbed BSA at equilibrium onto 6-layered and un-layered surfaces are $1.5\ \mathrm{mg\ m^{-2}}$ and $3.0\ \mathrm{mg\ m^{-2}}$, respectively. Thus, polyelectrolyte deposition suppresses BSA adsorption. This occurs because the enhanced hydrophilicity imparted by the polyelectrolyte multilayer lowers the hydrophobic interaction between the membrane surface and the BSA.

Fig. 12 shows the relationship between the frequency shift, $\Delta f$, and the dissipation shift, $\Delta D$, obtained from the QCM-D measurement. The dissipation shift increases as the absolute value of the frequency shift (which is proportional to the amount of adsorption) increases. Here, smaller local slope of the plots represents rigid deposition and higher local slope represents soft deposition onto the polymer surface [44]. As shown by the differences in slope between the un-layered and 6-layered cases (the 6-layer surface exhibits the higher slope), BSA forms a rigid adsorption layer on an un-layered surface, while adsorbing in a soft layer on a polyelectrolyte multilayered surface. This indicates that, as BSA adsorbs onto the polyamide surface, it readily undergoes a conformational change due to the strong hydrophobic interaction between BSA and polyamide. On the other hand, BSA undergoes little conformational change following adsorption to the hydrophilic polyelectrolyte surface due to the weak interaction. This weak interaction is the reason why the LbL assembly on the membrane surface can reduce the membrane fouling.
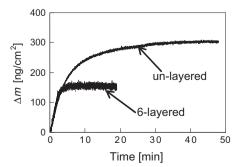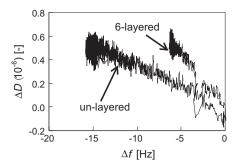
### 4. Conclusion

In this study, the antifouling property of polyelectrolyte multilayered RO membranes was investigated. Polyelectrolytes were successfully deposited onto the RO membrane via LbL assembly. The polyelectrolyte multilayer improved the antifouling property of RO membrane while retaining high NaCl rejection. The antifouling capability increased with increasing layer number due to enhanced hydrophilicity on the membrane surface and smoothed surface morphology. Under the conditions of the BSA fouling experiment, the optimal layer number (in terms of water permeability) was found to be 4. QCM-D measurements revealed that the amount of adsorbed BSA was much lower for polyelectrolyte multilayered surfaces than for polyamide layered surfaces. In addition, the ability of protein to adsorb and undergo a conformational change was reduced on polyelectrolyte multilayered surfaces due to their enhanced hydrophilicity. Based on these investigations, we conclude that LbL assembly is a promising surface modification candidate for improving the antifouling property of RO membranes.

### References

[1] M. Elimelech, X. Zhu, A.E. Childress, S. Hong, Role of membrane surface morphology in colloidal fouling of cellulose acetate and composite aromatic polyamide reverse osmosis membranes, J. Membr. Sci. 127 (1997) 101–109.
[2] E.M. Vrijenhoek, S. Hong, M. Elimelech, Influence of membrane surface properties on initial rate of colloidal fouling of reverse osmosis and nanofiltration membranes, J. Membr. Sci. 188 (2001) 115–128.
[3] Q. Li, Z. Xu, I. Pinnau, Fouling of reverse osmosis membranes by biopolymers in wastewater secondary effluent: role of membrane surface properties and initial permeate flux, J. Membr. Sci. 290 (2007) 173–181.
[4] A.E. Childress, M. Elimelech, Effect of solution chemistry on the surface charge of polymeric reverse osmosis and nanofiltration membranes, J. Membr. Sci. 119 (1996) 253–268.
[5] C. Jarusutthirak, G. Amy, Understanding soluble microbial products (SMP) as a component of effluent organic matter (EfOM), Water Res. 41 (2007) 2787–2793.
[6] C. Jarusutthirak, G. Amy, J.P. Croue, Fouling characteristics of wastewater effluent organic matter (EfOM) isolates on NF and UF membranes, Desalination 145 (2002) 247–255.
[7] D.J. Barker, D.C. Stuckey, A review of soluble microbial products (SMPs) in wastewater treatment systems, Water Res. 33 (1999) 3063–3082.
[8] R.P. Schneider, L.M. Ferreira, P. Binder, J.R. Ramos, Analysis of foulant layer in all elements of an RO train, J. Membr. Sci. 261 (2005) 152–162.
[9] E. Matthiasson, The role of macromolecular adsorption in fouling of ultrafiltration membranes, J. Membr. Sci. 16 (1983) 23–36.
[10] G. Kang, M. Liu, B. Lin, Y. Cao, Q. Yuan, A novel method of surface modification on thin-film composite reverse osmosis membrane by grafting poly(ethylene glycol), Polymer 48 (2007) 1165–1170.
[11] G. Kang, H. Yu, Z. Liu, Y. Cao, Surface modification of a commercial thin film composite polyamide reverse osmosis membrane by carbodiimide-induced grafting with poly(ethylene glycol) derivatives, Desalination 275 (2011) 252–259.
[12] X. Wei, Z. Wang, J. Chen, J. Wang, S. Wang, A novel method of surface modification on thin-film-composite reverse osmosis membrane by grafting hydantoin derivative, J. Membr. Sci. 346 (2010) 152–162.
[13] S.S. Shiratori, M.F. Rubner, PH-dependent thickness behavior of sequentially adsorbed layers of weak polyelectrolytes, Macromolecules 33 (2000) 4213–4219.

**Fig. 11.** Amount of BSA adsorbed onto un-layered and 6-layered polyamide-coated QCM sensor as a function of time.

[14] G. Decher, Fuzzy nanoassemblies: toward layered polymeric multicomposites, Science 277 (1997) 1232–1237.

[15] D. Yoo, S.S. Shiratori, M.F. Rubner, Controlling bilayer composition and surface wettability of sequentially adsorbed multilayers of weak polyelectrolytes, Macromolecules 31 (1998) 4309–4318.

[16] L. Ouyang, R. Malaisamy, M.L. Bruening, Multilayer polyelectrolyte films as nanofiltration membranes for separating monovalent and divalent cations, J. Membr. Sci. 310 (2008) 76–84.

[17] R. Steitz, V. Leiner, R. Siebrecht, R.v. Klitzing, Influence of the ionic strength on the structure of polyelectrolyte films at the solid/liquid interface, Colloids Surf. A 163 (2000) 63–70.

[18] J.D. Mendelsohn, C.J. Barrett, V.V. Chan, A.J. Pal, A.M. Mayes, M.F. Rubner, Fabrication of microporous thin films from polyelectrolyte multilayers, Langmuir 16 (2000) 5017–5023.

[19] G. Ladam, P. Schaad, J.C. Voegel, P. Schaaf, G. Decher, F. Cuisinier, In situ determination of the structural properties of initially deposited polyelectrolyte multilayers, Langmuir 16 (2000) 1249–1255.

[20] L. Liu, S. Guo, J. Chang, C. Ning, C. Dong, D. Yan, Surface modification of polycaprolactone membrane via layer-by-layer deposition for promoting blood compatibility, J. Biomed. Mater. Res. B: Appl. Biomater. 87 (2008) 244–250.

[21] D. Yu, C. Jou, W. Lin, M. Yang, Surface modification of poly(tetramethylene adipate-co-terephthalate) membrane via layer-by-layer assembly of chitosan and dextran sulfate polyelectrolyte multiplayer, Colloids Surf. B: Biointerfaces 54 (2007) 222–229.

[22] Q. Tan, J. Ji, M.A. Barbosa, C. Fonseca, J. Shen, Constructing thromboresistant surface on biomedical stainless steel via layer-by-layer deposition anticoagulant, Biomaterials 24 (2003) 4699–4705.

[23] W. Jin, A. Toutianoush, B. Tieke, Use of polyelectrolyte layer-by-layer assemblies as nanofiltration and reverse osmosis membranes, Langmuir 19 (2003) 2550–2553.

[24] L. Krasemann, A. Toutianoush, B. Tieke, Self-assembled polyelectrolyte multilayer membranes with highly improved pervaporation separation of ethanol/water mixtures, J. Membr. Sci. 181 (2001) 221–228.

[25] G. Zhang, H. Yan, S. Ji, Z. Liu, Self-assembly of polyelectrolyte multilayer pervaporation membranes by a dynamic layer-by-layer technique on a hydrolyzed polyacrylonitrile ultrafiltration membrane, J. Membr. Sci. 292 (2007) 1–8.

[26] N.A. Kotov, S. Magonov, E. Tropsha, Layer-by-layer self-assembly of alumosilicate-polyelectrolyte composites: mechanism of deposition, crack resistance, and perspectives for novel membrane materials, Chem. Mater. 10 (1998) 886–895.

[27] R. Malaisamy, M.L. Bruening, High-flux nanofiltration membranes prepared by adsorption of multilayer polyelectrolyte membranes on polymeric supports, Langmuir 17 (2005) 10587–10592.

[28] K. Tung, Y. Jean, D. Nanda, K. Lee, W. Hung, C. Lo, J. Lai, Characterization of multilayer nanofiltration membranes using positron annihilation spectroscopy, J. Membr. Sci. 343 (2009) 147–156.

[29] M. Müller, T. Rieser, K. Lunkwitz, J. Meier-Haack, Polyelectrolyte complex layers: a promising concept for antifouling coatings verified by in-situ ATR–FTIR spectroscopy, Macromol. Rapid Commun. 20 (1999) 607–611.

[30] M. Müller, T. Rieser, P.L. Dubin, K. Lunkwitz, Selective interaction between proteins and the outermost surface of polyelectrolyte multilayers: influence of the polyanion type, pH and salt, Macromol. Rapid Commun. 22 (2001) 390–395.

[31] J. Wang, Y. Yao, Z. Yue, J. Economy, Preparation of polyelectrolyte multilayer films consisting of sulfonated poly(ether ether ketone) alternating with selected anionic layers, J. Membr. Sci. 337 (2009) 200–207.

[32] C. Ba, D.A. Ladner, J. Economy, Using polyelectrolyte coatings to improve fouling resistance of a positively charged nanofiltration membrane, J. Membr. Sci. 347 (2010) 250–259.

[33] C. Bellona, J.E. Drewes, The role of membrane surface charge and solute physicochemical properties in the rejection of organic acids by NF membranes, J. Membr. Sci. 249 (2005) 227–234.

[34] M. Rodahl, F. Hook, A. Krozer, B. Kasemo, P. Breszinsky, A quartz crystal microbalance setup for frequency and Q factor measurements in gaseous and liquid environments, Rev. Sci. Instrum. 66 (1995) 3924–3930.

[35] K.P. Lee, T.C. Arnot, D. Mattia, A review of reverse osmosis membrane materials for desalination—development to date and future potential, J. Membr. Sci. 370 (2011) 1–22.

[36] J.E. Cadotte, Reverse Osmosis Membrane, Patent Application No. 4039440, 1977.

[37] S. Kwak, Relationship of relaxation property to reverse osmosis permeability in aromatic polyamide thin-film-composite membranes, Polymer 40 (1999) 6361–6368.

[38] G. Sauerbrey, Verwendung von Schwingquartzen zur Wägung dünner Schichten und zur Mikrowägung, Z. Phys. 155 (1959) 206–222.

[39] Z. Adamczyk, B. Zembala, P. Warszynski, B. Jachimska, Characterization of polyelectrolyte multilayers by the streaming potential method, Langmuir 20 (2004) 10517–10525.

[40] B. Schwarz, M. Schönhoff, Surface potential driven swelling of polyelectrolyte multilayers, Langmuir 18 (2002) 2964–2966.

[41] S. Schwarz, K.J. Eichhorn, E. Wischerhoff, A. Laschewesky, Polyelectrolyte adsorption onto planar surfaces: a study by streaming potential and ellipsometry measurements, Colloids Surf. A 159 (1999) 491–501.

[42] B. Schoeler, G. Kumaraswamy, F. Caruso, Investigation of the influence of polyelectrolyte charge density on the growth of multilayer thin films prepared by the layer-by-layer technique, Macromolecules 35 (2002) 889–897.

[43] T.J. Su, J.R. Lu, R.K. Thomas, Z.F. Cui, J. Penfold, The conformational structure of bovine serum albumin layers adsorbed at the silica–water interface, J. Phys. Chem. B 102 (1998) 8100–8108.

[44] T. Indesta, J. Laineb, K.S. Kleinscheka, L.F. Zemljic, Adsorption of human serum albumin (HSA) on modified PET films monitored by QCM-D XPS and AFM, Colloids Surf. A: Physicochem. Eng. Aspects 360 (2010) 210–219.